PROPOSALS TO ACCOUNT FOR THE ANGLE OF SEISMIC INCIDENCE WHEN APPLYING THE PEER-PBEE METHODOLOGY

DESPOINA SKOULIDOU
PhD candidate
FEUP

XAVIER ROMÃO
Assistant Professor
FEUP

ABSTRACT

The paper discusses the overall effect of the angle of seismic incidence during the seismic safety assessment of reinforced concrete buildings employing state-of-the-art methods of analysis, and provides proposals on how to account for this effect. Particularly, the Performance Based Earthquake Engineering (PBEE) methodology developed by the Pacific Earthquake Engineering Research (PEER) Centre is applied to six reinforced concrete buildings and the effect of the angle of seismic incidence is evaluated in all relevant stages of the procedure. The PEER-PBEE methodology provides a general framework for the probabilistic assessment of the seismic performance of individual buildings, it comprises four stages of analyses, and yields results that are of interest both for practitioner engineers and stakeholders. The angle of seismic incidence is involved in the second stage of the framework, which includes the structural analysis of the building, and primarily affects the resulting engineering demand parameters. Subsequently, the propagation of the effect of the angle of seismic incidence is also examined in the following two stages of the framework, which involve the damage and the loss analysis of the building. Different metrics of building performance are analysed in each stage of the framework, including two engineering demand parameters (in the structural analysis stage), the probability of collapse (in the damage analysis stage) and the expected annual loss of the building (in the loss analysis stage). Proposals to account for the angle of seismic incidence are provided based both on results obtained for each individual stage of the framework, as well as on the overall assessment procedure.

KEYWORDS: angle of seismic incidence; probabilistic seismic analysis; ground motion group size; RC buildings.

1. INTRODUCTION

The Performance-Based Earthquake Engineering (PBEE) framework for the probabilistic assessment of the seismic performance of a building [1] allows the consideration of various sources of uncertainty. Common sources are those associated with the seismic input, expressed by the seismic hazard uncertainty [2] and the record-to-record variability [3], the structural modelling, such as the variability of geometric properties and material constitutive laws [1], [3], the damage definitions and the economic losses [4]. It is known that accounting for such uncertainties changes seismic demand, the parameters of fragility functions and the associated seismic risk [5], as well as the seismic losses [6].

An additional source of uncertainty that has received less attention is that related with the angle of seismic incidence (ASI). The ASI is the direction of application of the seismic action on the structural model and its adequate selection is relevant when structural analyses involve three-dimensional models. Despite the early recognition of the ASI's importance [7], studies addressing its relevance in probabilistic terms are few so far. The idea of defining an adequate number of ground motions (GMs) and of ASIs to estimate inelastic demand with a predefined confidence level was suggested in [8]. In a loss assessment framework [9], the ASI was sampled from a uniform distribution and it was concluded that 20 ground motions applied along 5 random ASIs are adequate to account for the randomness of both the GMs and the ASI in the engineering demand parameters (EDP) estimates. The effect of the ASI was also included in a probabilistic framework involving Multidirectional Incremental Dynamic Analysis [10] and results suggested combining 30 GMs with an equal number of ASIs. In a recent study [11], the GM group size was seen to have a much larger effect than that of the ASI on location and variation measures of selected EDPs, thus suggesting that the contribution of the ASI could be ignored. Still, another study involving EDP distributions [13] showed that both the ASI and the GM group size have non-negligible effects. This summary of existing research shows that a variety of conclusions have been reached in the past. Consequently, different suggestions have been made about the effect of the ASI and on ways to account for this effect. However, no general agreement was found so far.

To provide further insights about the effect of the ASI on the probabilistic assessment of the seismic performance of buildings, the present study applies the PBEE methodology developed by the Pacific Earthquake Engineering Research (PEER) Centre to 6 reinforced concrete (RC) buildings and evaluates the effect of the ASI in several stages of the procedure. The PEER-PBEE framework has four stages of analyses and the ASI is explicitly involved in the second stage, which includes the structural analysis of the building. The effect of the ASI is then propagated to the last two stages of the procedure, the damage and the loss assessment. The effect of the ASI is evaluated in all three stages using appropriate metrics, such as selected EDPs for the structural analysis stage, the collapse risk for the damage assessment and the expected annual loss for the loss assessment. Since the structural analysis involves nonlinear dynamic analyses, the study integrates the effects of the ASI and of the GM group size. The results indicate that different metrics are influenced in a different level by the GM group size and the number of ASIs and that the effect of the ASI decreases when progressing through the stages of the framework.

2. PRESENTATION OF THE BUILDINGS AND STRUCTURAL MODELLING

Six RC buildings with masonry infilled frame systems are analysed. The buildings have low- to mid-rise configurations with and without in-plan irregularities. All buildings are located in Lisbon, Portugal, and are designed for gravity loads only. The plan view of a typical storey of the 3-storey (3-Ir), the 4-storey (4-Ir) and the 5-storey (5-Ir) irregular buildings is presented in Fig. 1a, along with design details. Similarly, the plan view of a typical story of the 3-storey (3-R), the 4-storey (4-R) and the 5-storey (5-R) regular buildings are also shown in Fig. 1b along with design details. The concrete strength and the steel yield strength are considered to be 25 MPa and 500 MPa, respectively.

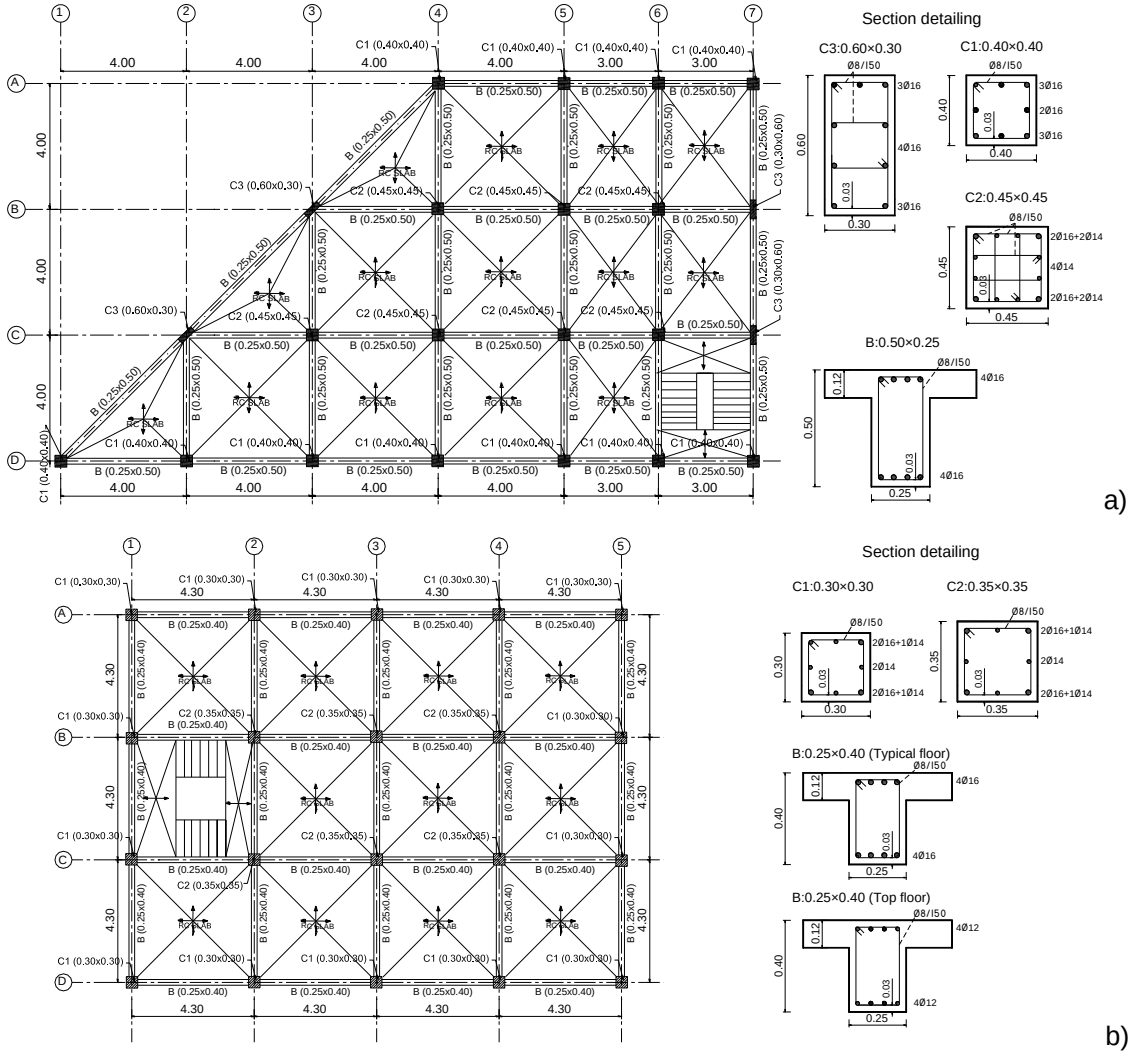

Fig. 1 – Plan view of a typical story of the 3-Ir, 4-Ir and 5-Ir buildings and design details (a) and plan view of a typical story of the 3-R, 4-R and 5-R buildings and design details (b)

All buildings are modelled in the OpenSees software [14] considering mean values of the material and geometrical properties. A lumped plasticity approach is adopted to simulate the inelastic behaviour of all structural elements. Phenomenological hysteresis laws are assigned to rotational springs located on both ends of all columns and beams to simulate inelastic flexural behaviour. Two independent springs are assigned to each end of the columns, one for each orthogonal direction, while one spring is assigned to each end of the beams modelling the in-plane flexural behaviour. Due to the nature of the selected inelastic modelling approach, no biaxial moment interaction or axial force moment interaction is considered when modelling the behaviour of columns.

Hysteretic flexural behaviour is simulated using the *hysteretic* material in OpenSees. The yielding moment (M_y) and the yielding rotation (θ_y) are determined according to [15]. The capping (θ_c) and post-capping (θ_{pc}) rotations are computed according to [16] and a final 20% residual moment (M_r) is considered at the ultimate rotation (θ_u) (see Fig. 2a). Stiffness, strength and unloading stiffness degradations are considered in the hysteresis curves. Each beam-column element is defined by a serial arrangement of the end springs connected to a linear elastic element. A stiffness modification factor equal to 10 is applied according to [17] to account for the effect of the series connection of the elements on the total stiffness of the element. For beam-column joints, rigid elastic elements are used with a length equal to half of the length of the corresponding perpendicular element. The occurrence of shear failure or beam-column joint failure are not modelled but can be

analysed in post-processing. Infills are considered in all peripheral frames and are modelled using two diagonal compression-only strut elements. The equivalent area of each strut is based on the maximum lateral force of the infill and on the masonry compressive strength [18]. The parameters obtained, i.e. the maximum stress (f_m) and strain, are used to define the masonry material with zero tensile strength simulated by the *Concrete01* constitutive model (Fig. 2b). The masonry compressive strength is equal to 3.10 MPa and all infills have a thickness of 0.15m. Additionally, a residual stress equal to 10% of the maximum stress is considered for numerical stability.

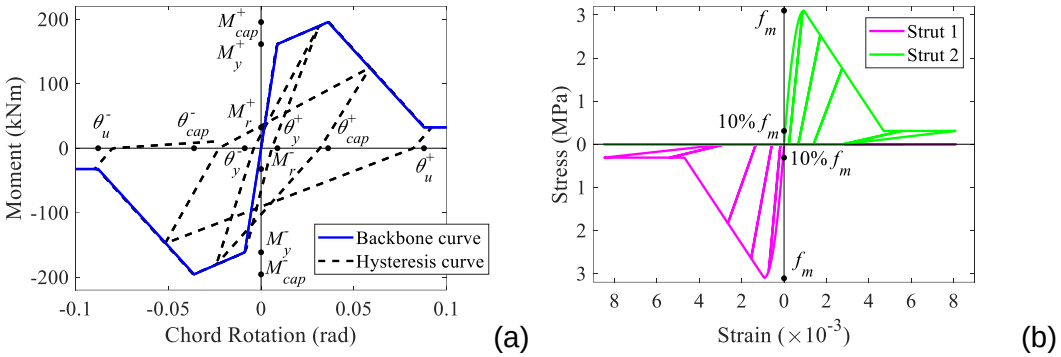

Fig. 2 – Moment-rotation backbone curve and hysteresis loop simulation for a column (a) and stress – strain relationship of the infill struts (in compression) in the diagonal direction (b)

A permanent load of 4 kN/m^2 is uniformly distributed on all slabs, additional to the slab self-weight. A uniform live load of 3 kN/m^2 is also assigned to all slabs, except to the top storey slabs, where the live load is 1 kN/m^2. Staircases are only modelled as permanent and live loads, which are then transferred to the supporting beams and applied uniformly. The corresponding loads are 7.75 kN/m and 8.60 kN/m for the permanent and the live loads, respectively. Masonry infills also load uniformly all peripheral frames with 7 kN/m. The fundamental periods of vibration of each building are presented in Table 1. The average of the first two periods of the infilled structure and of the first two periods of the bare structure T^* is also presented in Table 1 and is used for the GM selection. Defining T^* using periods of vibration of the bare structure is conceptually similar to accounting for the period elongation of the infilled building after yielding and failure of the infills.

Table 1 - First and second mode periods of vibration of the buildings

Periods (s)	**3-R**	**4-R**	**5-R**	**3-Ir**	**4-Ir**	**5-Ir**
T_1,T_2 (w infills)	0.31, 0.25	0.41, 0.31	0.52, 0.39	0.21, 0.15	0.29, 0.20	0.37, 0.26
T_1,T_2 (w/o infills)	0.73, 0.72	0.96, 0.93	1.18, 1.15	0.39, 0.35	0.55, 0.47	0.70, 0.60
T^*	0.50	0.66	0.82	0.27	0.38	0.48

3. SEISMIC HAZARD ANALYSIS AND GROUND MOTION SELECTION

The probabilistic seismic hazard analysis of the site is performed using OpenQuake [19] considering Lisbon, Portugal, as the benchmark site for all structures. The annual seismic hazard curve H_{IM} of the benchmark site is determined at T^* for each building and is shown in Fig 3a. Hazard disaggregation is then carried out for four probabilities of exceedance, i.e. 30%, 10%, 5% and 2% in 50 years, at T^* for each building The hazard disaggregation for the 30% in 50 years and for T^* = 0.66s is also shown in Fig. 3b. Four conditional spectra (CS) [20] are then constructed for each building, each one associated with one of the probabilities of exceedance. Figure 3c shows the CS for T^*=0.5s.

The GM selection is carried out using the SelEQ software [21] considering the CS as the target spectrum. Prior to this detailed procedure, a preliminary selection of GMs from the NGA database [22] is performed using seismological and strong motion parameters.

Next, 40 bi-directional GM records are selected based on the criteria and the objective function described in [21]. As a result, four groups of 40 bi-directional GMs are obtained for each building, one for each CS corresponding to the previously referred probabilities of exceedance of 30%, 10%, 5% and 2% in 50 years, e.g. see Fig. 3c for the 3-R building (T^*=0.5s) and 30% in 50 years. Each group of 40 bi-directional records is subsequently re-sampled to create groups of size n = 10, 15, 20, 25, 30 and 35. Specific provisions are considered to maintain the compatibility between each new group and the reference group of size 40 in terms of seismic input and 100 groups are obtained for each size n.

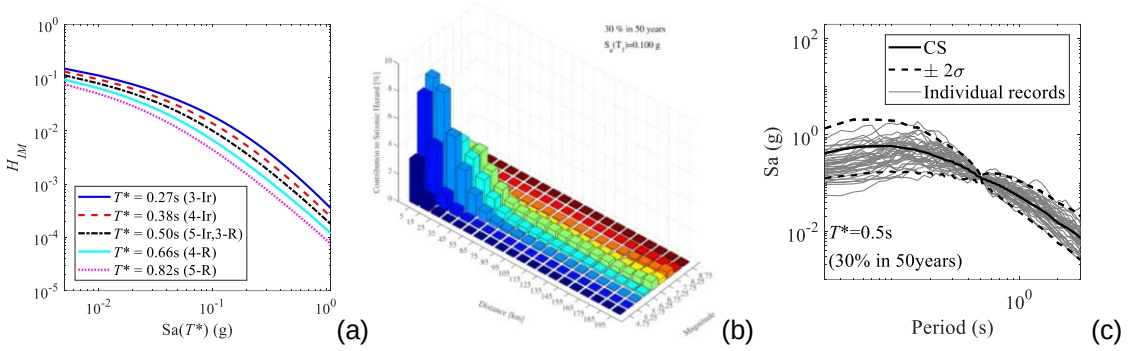

Fig. 3 – The CS and the geometric means of the 40 ground motions for the 3-R building

4. STRUCTURAL ANALYSIS

4.1. Probabilistic demand model

The six buildings presented in Section 2 are subjected to multi-stripe analysis [23] with the GM groups defined in Section 3. Following a procedure similar to that proposed in [24], the four groups, corresponding to the intensities of the previously referred probabilities of exceedance, are scaled up and down to cover a total of 20 intensities. Figure 4 shows a schematic representation of the scaled average geometric response spectra for the case of the 3-R building (T^*=0.5s).

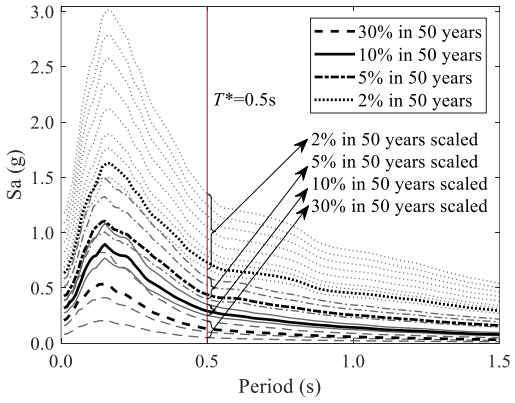

Fig. 4 – Average geometric response spectra of the 40 ground motions scaled for different intensities for the 3-R building (T^*=0.5s).

All six buildings are subsequently subjected to nonlinear dynamic analyses for the 20 intensity levels (stripes) with the 40 record pairs of each stripe applied along 12 ASIs. The considered ASIs range from 0° to 165° in steps of 15° and are considered to be equally likely. The sources of uncertainty considered in the structural response are then the result of the record-to-record variability and the ASI of each record. As referred before, 100 groups of GMs are considered for each size n to account for the record-to-record variability in different group sizes. All groups are also applied along different

numbers of ASIs, from 1 to 12. When a single ASI is used, the seismic action is applied along a direction coinciding with the structural axes of the building, i.e. all GMs of a group are applied along 0º. When multiple ASIs are used, the ASIs equidistantly cover the total angle range and the first ASI is always 0º. For instance, using two ASIs corresponds to angles 0º and 90º, while using three ASIs corresponds to angles 0º, 60º and 120º. The overall procedure leads to 100 groups for each combination of group size *n* and number of ASIs, thus providing adequate data for the statistical post processing of the results.

4.2. Effect of the ASI at the EDP level

The seismic demand distributions of the maximum interstorey drift ratio ISD and the peak floor acceleration PFA are analysed. The analysis of these EDPs is performed using two descriptive statistics, i.e. the median and the standard deviation (std), to estimate the central tendency and the dispersion of the EDP distributions. The statistics obtained using a particular combination of *n* and number of ASIs are estimates of the true, yet unknown, statistics due to the finite number of ASIs and size *n*. Furthermore, the statistic estimates obtained from groups of 40 GMs applied along all 12 ASIs are considered as the reference values of the respective statistics and are used herein to compare the previously defined estimates. Selected results of the statistical analyses are presented in Figs. 5 to 7 to show the effect of the ASI and the size *n* on each statistic of the two EDPs. The 100 statistic estimates, obtained using a particular combination of *n* and ASI, are normalised by the reference value of the respective statistic and a kernel distribution is then fitted to them. Violin plots are used to better visualise the obtained distributions.

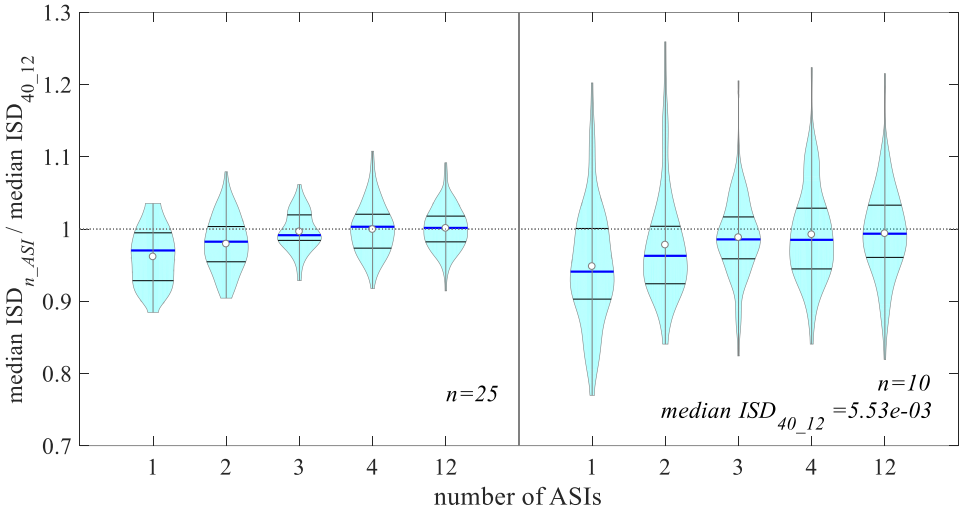

Fig. 5 – Violin plots of the median ISD logarithms for *n*=25 and *n*=10 and selected ASIs (results obtained from the 4-R building and the 10% in 50 years probability of exceedance)

Figure 5 shows the violin plots of the normalised median ISD of the 4-R building obtained using combinations of a large *n* (*n*=25) and selected ASIs (left) and combinations of a small *n* (*n*=10) and selected ASIs (right). Similarly, Fig. 6 shows the violin plots of the normalised median PFA of the 3-R building obtained using combinations of a large *n* (*n*=25) and selected ASIs (left) and combinations of a small *n* (*n*=10) and selected ASIs (right). Since no significant differences could be found between the case using 12 ASIs and the cases using 4 to 12 ASIs, results involving 5 to 11 ASIs were omitted. It is observed that, for both EDPs, using only 1 ASI can lead to a larger variability of the median when compared to the case using all 12 ASIs. This variability decreases when 2 ASIs are used and, in most of the cases, using 3 or more ASIs makes little difference. The effect of the size *n* on the variability, on the other hand, is much larger than that of the ASI, for both EDPs, and leads to a larger decrease of the variability as *n* increases. Another important effect of using only 1 ASI is the shift of the whole distribution with respect to the reference value. This shift is observed in both EDPs and can lead to either

an under- or overestimation (not shown herein) of the demand and it can be effectively corrected for the larger sizes *n* by using at least 2 ASIs. For sizes *n* smaller than 15 on the other hand the variability and the bias introduced by the small size *n* are not always effectively corrected by increasing the number of ASIs, e.g. see Fig. 6 (right).

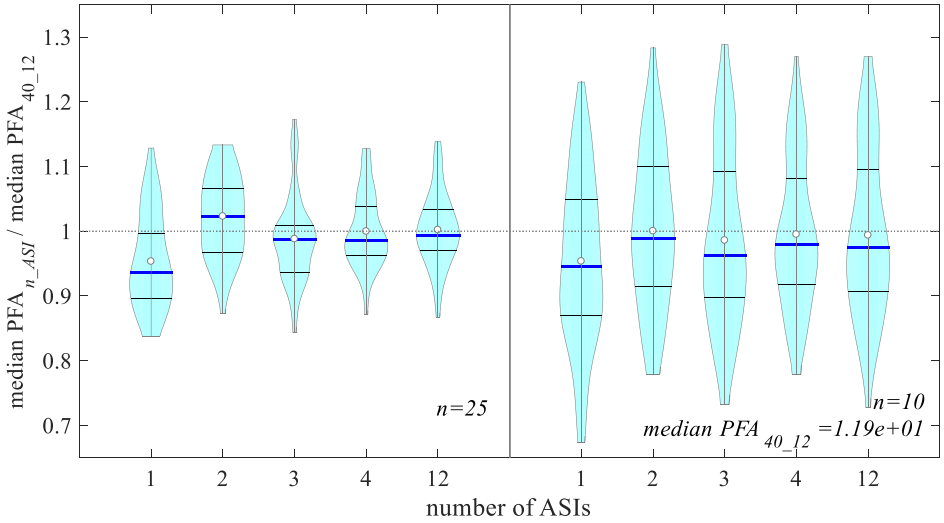

Fig. 6 – Violin plots of the median PFA logarithms for *n*=25 and *n*=10 and selected ASIs (results obtained from the 3-R building and the 5% in 50 years probability of exceedance)

In order to discuss the effect of the ASI and *n* on the std of the ISD, Fig. 7 shows the violin plots of the normalised std of the ISD logarithms of the 5-R building obtained using combinations of a large size *n* (*n*=25) and selected ASIs (left) and combinations of a small size *n* (*n*=10) and selected ASIs (right). A larger variation is observed for the std when compared to that of the median values presented in Figs. 6 and 7. Still, effects similar to those observed for the median values are seen here as well, with the size *n* having a larger influence on the variability of the kernel distribution, while the ASI has a smaller effect on the variability but also affects the central values. The increased variability and bias can be corrected by using more than 15 ground motions and more than 3 ASIs in most of the cases. Similar results were found for the std of the PFA.

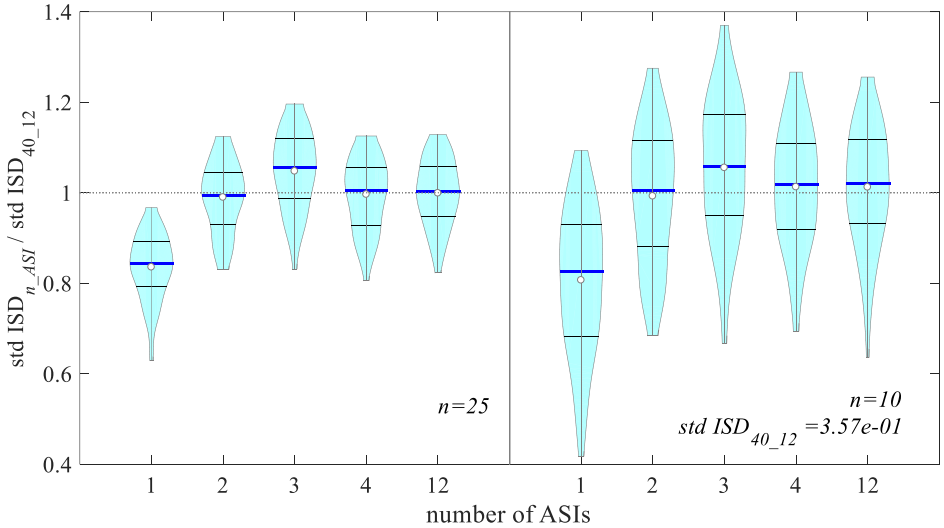

Fig. 7 – Violin plots of the std ISD logarithms for for *n*=25 and *n*=10 and selected ASIs (results obtained from the 5-R building and the 5% in 50 years probability of exceedance)

5. DAMAGE ANALYSIS

5.1. Capacity, collapse fragility and risk model

The probability of collapse and the intermediate step of the PEER-PBEE framework, the collapse risk, are examined in this stage. Collapse of the buildings is associated to the occurrence of one of the following three conditions: 1) exceedance of the ultimate chord rotation in a column (flexural failure), 2) shear failure in a column or 3) numerical failure of the model. The ultimate chord rotation and shear capacities involve component-level failure mechanisms indicating the loss of load bearing capacity of a column and are evaluated for each column using the models proposed in [25] and [26], respectively. Numerical failure occurs when interstorey drifts increase without bound and lead to non-convergence of the numerical algorithm, thus terminating the analysis. The development of a soft storey (a system-level failure mechanism) is a typical example that often leads to numerical failure since it usually generates dynamic instability of the model. The modelling approaches selected to simulate the nonlinear behaviour of the buildings (see Section 2) are able to prevent early numerical failures and ensure that the analysis will converge even for cases involving a large spread of plasticity.

Collapse risk, considered herein as being equivalent to the mean annual collapse rate λ_C [1] of a given structure, is defined by the integral:

$$\lambda_C = \int_0^\infty \mathrm{P}\left(\mathrm{C}|\mathrm{IM}=im\right)\left|dH_{IM}(im)\right| \tag{1}$$

where $\mathrm{P}\left(\mathrm{C}|\mathrm{IM}=im\right)$ and $dH_{IM}(im)$ are the collapse fragility and the derivative of the annual seismic hazard curve, respectively, for an intensity IM equal to *im*. The collapse fragility represents the probability of collapse $\mathrm{P}(\mathrm{C})$ of the structure given the *im*

$$\mathrm{P}\left(\mathrm{C}|\mathrm{IM}=im\right)=\Phi\left(\frac{\log(im/\theta_C)}{\beta_C}\right) \tag{2}$$

where Φ is the standard normal distribution function with parameters $\log(\theta_C)$ and β_C, obtained herein using the EDP-based approach suggested in [27].

5.2. Effect of the ASI on the collapse fragility and collapse risk

The overall procedure leads to 100 fragility curves and subsequently to 100 risk values for each combination of GM group size *n* and number of ASIs. A preliminary evaluation of the effect of the ASI is performed by fitting a kernel cumulative distribution function (KCDF) to the 100 estimates of each parameter, i.e. θ_C, β_C and λ_C, and by comparing KCDFs obtained using combinations of *n* and ASI by varying the number of ASIs. An example of these results is shown in Fig. 8, where the KCDFs of θ_C, β_C and λ_C for combinations of *n*=25 and ASIs 1 to 12 and for the 5-Ir building are presented. It is observed that, given the size *n*, the variability of all parameters is not significantly influenced by the use of different number of ASIs (i.e. the KCDFs are parallel and relatively close to each other), except for the case involving only 1 ASI. It is also noted that, when increasing the number of ASIs, the distribution of θ_C oscillates around the more refined case (12 ASIs). Again, the largest shift (always left-ward for the 5-Ir building) occurs for the case where only 1 ASI is involved. Similar remarks can be made for the distribution of β_C with respect to the number of ASIs, i.e. the shift of the distribution of β_C when a different number of ASIs is involved. Nevertheless, the shift in this case appears to be much smaller. Finally, with respect to λ_C, which combines the effects of

[1] Assuming that both hazard and fragility are memoryless, collapse can be considered to be a Poisson process and the probability of collapse, i.e. the risk of collapse, can be derived by: $P_C = 1 - e^{-\lambda_C}$, which in case of small collapse rates, can be considered equal to the collapse rate without significant error.

the previous two parameters and of the seismic hazard, the number of ASIs and the size *n* appear to have similar effects on the KCDFs as those discussed for θ_C, suggesting that these effects propagate to $\hat{\lambda}_C$.

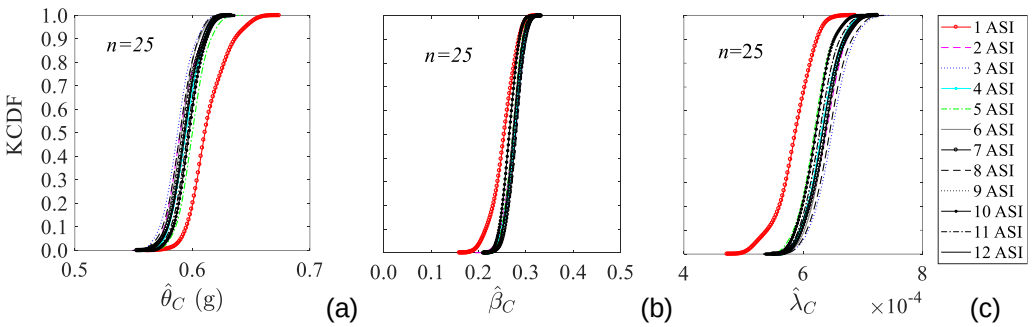

Fig. 8 – KCDFs of θ_C, β_C and $\hat{\lambda}_C$ of the 5-Ir building for all GM groups of *n* equal to 25 and for 1 to 12 ASIs

As for the EDP statistics, and as explained in Section 4, the obtained risk values are estimates of the true risk, while the risk values determined using 40 GMs and 12 ASIs for each building are used as the reference values. Even though the variation of $\hat{\lambda}_C$ is only marginally influenced when the effect of the number of ASIs is neglected (i.e. when considering only 1 ASI), the median $\hat{\lambda}_C$ may experience a much larger bias in that case. To illustrate the consequences of this observation and particularly of this effect combined with the variation due to the finite GM group size *n*, Fig. 9 shows the boxplots of the distribution of the 100 $\hat{\lambda}_C$ normalized values obtained for each GM group size *n* and for three specific cases of the number of ASIs, for the 5-Ir building. The size *n* is seen to have a much larger effect on the variation, while the number of ASIs affects the central values of the distribution. Small sizes lead to high variability, and consequently to large over- or underestimation of the reference value. Increasing the number of ASIs doesn't always improve the results in these cases. Therefore, the use of more than 15 GMs is suggested. For larger sizes *n*, the variation around the median $\hat{\lambda}_C$ reduces significantly. Neglecting the effect of the ASI, however, results in a variation of $\hat{\lambda}_C$ around a biased median $\hat{\lambda}_{C(n\_1)}$, and leads to larger levels of over- or underestimation with respect to the reference value. Although considering 1 ASI is insufficient to obtain an unbiased estimate of the collapse risk, with just 2 ASIs (0° and 90°) this bias appears to be eliminated.

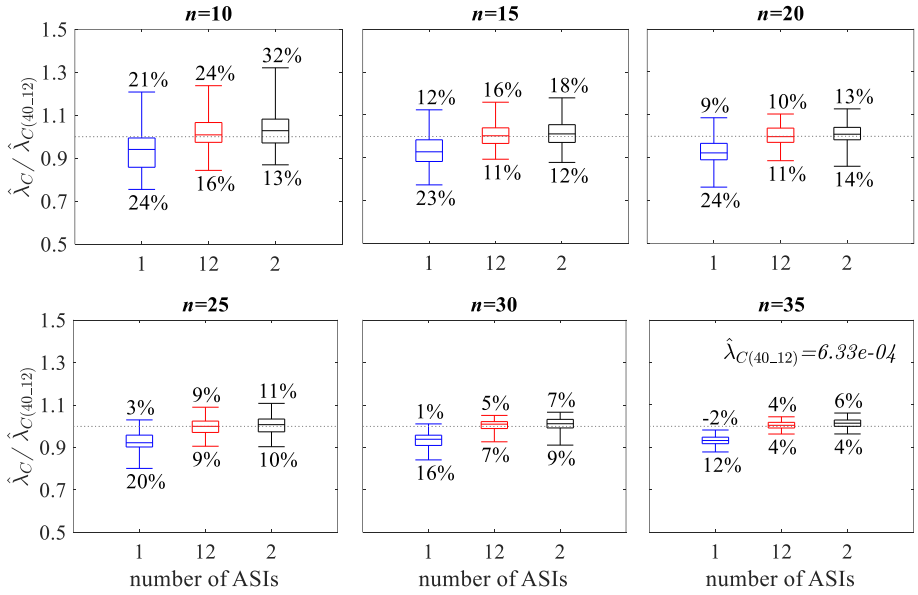

Fig. 9 – Boxplots of $\hat{\lambda}_{C(n\_1)}$, $\hat{\lambda}_{C(n\_2)}$, $\hat{\lambda}_{C(n\_12)}$ normalized by the $\hat{\lambda}_{C(40\_12)}$ for the 5-Ir building.

6. LOSS ANALYSIS

6.1. Fragility and cost data

The end product of the framework is the determination of the probability of exceedance of a decision variable DV. The DVs usually considered are the economic losses due to the repair of the structure, casualties and downtime. Due to difficulties in defining the last two components, only the first one is examined herein and corresponds to the direct economic losses *L*. Furthermore, since the purpose of the study is to determine the effect of the input seismic action, no uncertainty is considered in the economic losses and thus only the expected value of *L*, E(*L*), is determined. The E(*L*|IM), which represents the E(*L*) conditional to a given IM intensity level is defined by

$$\begin{aligned} \mathrm{E}(L \mid \mathrm{IM}_m) = \mathrm{E}(L \mid \mathrm{NC} \cap \mathrm{R}, \mathrm{IM}_m)\mathrm{P}(\mathrm{NC} \cap \mathrm{R} \mid \mathrm{IM}_m) + \\ \mathrm{E}(L \mid \mathrm{NC} \cap \mathrm{D}, \mathrm{IM}_m)\mathrm{P}(\mathrm{NC} \cap \mathrm{D} \mid \mathrm{IM}_m) + \mathrm{E}(L \mid \mathrm{C}, \mathrm{IM}_m)\mathrm{P}(\mathrm{C} \mid \mathrm{IM}_m) \end{aligned} \quad (3)$$

where $\mathrm{E}(L \mid \mathrm{NC} \cap \mathrm{R}, \mathrm{IM}_m)$ is the expected loss in the building given that no collapse has occurred and the building can be repaired, given the occurrence of the seismic intensity IM_m. The term $\mathrm{E}(L \mid \mathrm{NC} \cap \mathrm{D}, \mathrm{IM}_m)$ is the expected loss in the building given that no collapse has occurred and the building needs to be demolished, given the occurrence of the seismic intensity IM_m, and $\mathrm{E}(L \mid \mathrm{C}, \mathrm{IM}_m)$ is to the expected loss of the building when collapse occurs at the IM_m intensity. The expected loss of having to demolish and rebuild the building as well as the expected loss of the collapsed building are taken equal to the replacement cost of the building, which is considered to be 20% more than the cost of new construction. The weighting factors attributed to each cost-related component in Eq. (3) are $\mathrm{P}(\mathrm{NC} \cap \mathrm{R} \mid \mathrm{IM}_m)$, the probability that the building can be repaired given that no collapse has occurred at the seismic intensity IM_m, $\mathrm{P}(\mathrm{NC} \cap \mathrm{D} \mid \mathrm{IM}_m)$, the probability that the building should be demolished given that no collapse has occurred at the seismic intensity IM_m, and $\mathrm{P}(\mathrm{C} \mid \mathrm{IM}_m)$, the probability of collapse of the building given the intensity IM_m, defined in Section 5. Finally, the convolution of Eq. (3) with the seismic hazard curve presented in Section 3 leads to the expected annual loss (EAL):

$$\mathrm{E}(L) = \sum_m \mathrm{E}(L \mid \mathrm{IM}_m)\,\mathrm{p}(\mathrm{IM}_m) \quad (4)$$

The damageable building components that are considered in the present study are those presented in Table 2 along with references for the fragility functions and for the cost data.

Table 2 – List of damageable components with fragility function parameters and loss data

Component	Fragility function parameters		Cost reference
	EDP used	Reference	
Columns	Rot (rad)	[28],[29]	Expert ellicitation
Beams	Rot (rad)	[28],[29]	
Infill walls	ISD	[30]	
Doors	ISD	[30]	
Windows	ISD	[30]	
Suspended ceiling	PFA (g)	[1]	
Stairs	ISD	[1]	
Electrical wiring	ISD	Expert ellicitation	
Piping utilities	ISD	Expert ellicitation	

6.2. Effect of the ASI on the expected loss

Figure 10 presents an overview of the obtained losses by showing the total expected losses against the seismic intensity for building 3-R, considering all 100 groups of size

n=20 and ASI=1 (a) and ASI=12(b). These expected losses are normalised to the total cost of the building. Disaggregated losses, i.e. structural (Repair struct), non-structural (Repair NonStruct), collapse and demolition are also presented in Fig. 10 to highlight the contribution of the different components. Total repair loss is determined by summing the repair costs due to structural and non-structural elements. No noticeable difference is observed on the variability of the expected costs of the different components as a result of using two different number of ASIs. Still, it is noted that the largest variability is observed for the loss due to collapse, while the lowest variability is that of the repair cost of structural elements. Regarding the total loss, a moderate variability is observed, which doesn't seem to vary for the different number of ASIs.

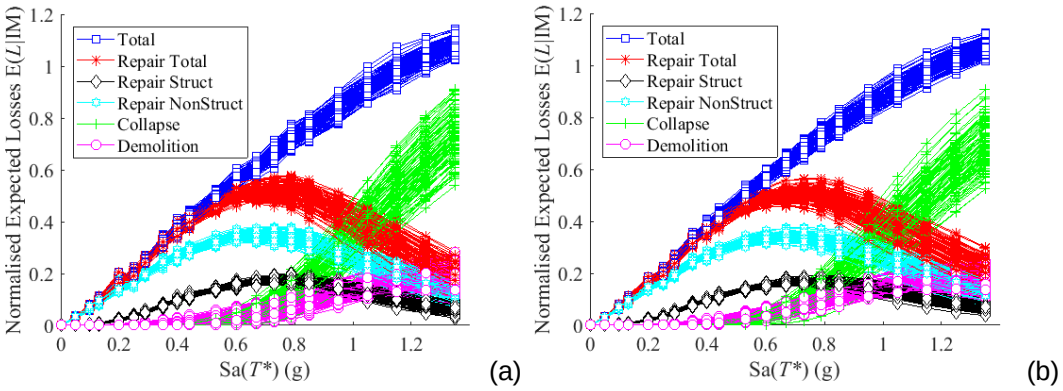

Fig.10 – Expected loss of the 3-R building as a function of the GM intensity, normalised by the cost of the new building for the 100 groups of size 20 and for ASI=1 (a) and ASI=12 (b)

Finally, the effect of the ASI and of the size *n* on the EAL is illustrated in Fig. 11. The figure shows the median EAL of all combinations of *n* with ASI for the 5-R building, represented with the bar plots, as well as the variation obtained due to the 100 groups of GMs for each combination. The presented EALs are normalised to the total cost of the building. The influence of the size *n* on the variability of the results is also present in this stage of the analysis, thus highlighting the effect of propagating the corresponding uncertainty. Nonetheless, a much lower level of variability can be seen for the EAL, with the under- or over estimation being always lower than 15% of the reference value, even for the smallest size *n*. The effect of the ASI appears to be negligible when estimating the EAL, thus using only 1 ASI appears to be adequate.

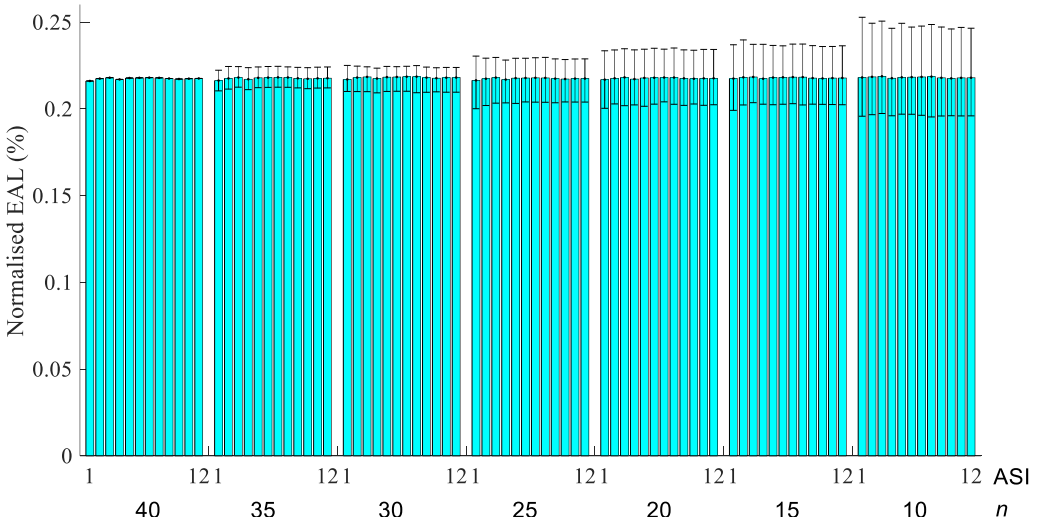

Fig.11 – Median EAL and variability of the 5-R building for all combinations of *n* with ASI.

7. DISCUSSION AND CONCLUSIONS

The effect of the number of ASIs and of the GM group size was examined in the context of the PEER-PBEE framework. Six buildings were analysed according to the PEER-PBEE procedure and the effect of the previously mentioned parameters was determined on the outcomes of each stage of the framework. The effect of the ASI was seen to decrease when progressing through the stages of the framework. As such, the use of only 1 ASI was seen to be adequate to estimate the EAL, 2 ASIs were found to be enough to estimate collapse risk and more than 2 ASIs were seen necessary to estimate most of the EDP distributions. The GM group size was shown to have a larger effect, when compared to that of the ASI, and the use of at least 20 GMs was suggested to reduce the variability of the results in all stages of the framework.

8. ACKNOWLEDGEMENTS

The authors would like to thank José Paupério, civil engineer at Pemi – Engenharia & Construção, Lda, and Miguel Santos, civil engineer and general manager at Cacao Civil Engineering, Lda, for providing the detailed component cost data that were used for the loss analysis. Financial support of the Portuguese Foundation for Science and Technology (FCT), through the PhD grant of the first author (PD/BD/113681/2015), is gratefully acknowledged. Finally, authors also acknowledge the financial support of UID/ECI/04708/2019 - CONSTRUCT - Instituto de I&D em Estruturas e Construções funded by national funds through the FCT/MCTES (PIDDAC).

9. REFERENCES

[1] FEMA P-58. Seismic performance assessment of buildings, volume III, Federal Emergency Management Agency 2012, Washington, D.C.
[2] Abrahamson NA and Bommer JJ. Probability and uncertainty in seismic hazard analysis. *Earthquake spectra* 2005; 21(2):603-607.
[3] Haselton CB, Baker JW, Bozorgnia Y, Goulet CA, Kalkan E, Luco N, Shantz T, Shome N, Stewart JP, Tothong P, Watson-Lamprey J and Zareian F. Evaluation of ground motion selection and modification methods: Predicting median interstory drift response of buildings. PEER 2009 (Technical Report 2009/01).
[4] Franchin P, Ragni L, Rota M and Zona A. Modelling uncertainties of Italian code-conforming structures for the purpose of seismic response analysis. *Journal of Earthquake Engineering* 2018; 22(sup2):1964-1989.
[5] Lee TH and Mosalam KM. Probabilistic seismic evaluation of reinforced concrete structural components and systems. PEER Report 2006. PEER 2006/04.
[6] Liel AB, Haselton CB, Deierlein GG and Baker JW. Incorporating modeling uncertainties in the assessment of seismic collapse risk of buildings. *Structural Safety* 2009; 31(2):197-211.
[7] Bradley BA and Lee DS. Accuracy of approximate methods of uncertainty propagation in seismic loss estimation. *Structural Safety* 2010; 32(1):13-24.
[8] Penzien J and Watabe M. Characteristics of 3-D earthquake ground motions. *Earthquake Engineering & Structural Dynamics* 1974; 3(4):365–73.
[9] Rigato AB and Medina RA. Influence of angle of incidence on seismic demands for inelastic single-storey structures subjected to bi-directional ground motions. *Engineering Structures* 2007; 29(10):2593–2601.
[10] Lagaros ND. The impact of the earthquake incident angle on the seismic loss estimation. *Engineering Structures* 2010; 32(6):1577–1589.
[11] Lagaros ND. Multicomponent incremental dynamic analysis considering variable incident angle. *Structure and Infrastructure Engineering* 2010; 6(1–2):77–94.
[12] Giannopoulos D and Vamvatsikos D. Ground motion records for seismic performance assessment: To rotate or not to rotate? *Earthquake Engineering & Structural Dynamics* 2018; 47(12):2410-2425.

[13] Skoulidou D and Romão X. Does the angle of seismic incidence affect inelastic seismic demand? A probabilistic point of view. In the 16th European Conference on Earthquake Engineering 2018, Thessaloniki, Greece.
[14] McKenna F and Fenves GL. Opensees 2.5.0, Computer Software. UC Berkeley, Berkeley (CA) 2011. http://opensees.berkeley.edu
[15] Panagiotakos TB and Fardis MN. Deformations of reinforced concrete members at yielding and ultimate. *Structural Journal* 2001; 98(2):135-148.
[16] Haselton CB, Goulet CA, Mitrani-Reiser J, Beck JL, Deierlein GG, Porter KA and Taciroglu E. An assessment to benchmark the seismic performance of a code-conforming reinforced-concrete moment-frame building. Pacific Earthquake Engineering Research Center, 2008 (2007/1).
[17] Zareian F and Medina RA. A practical method for proper modeling of structural damping in inelastic plane structural systems. *Computers & structures* 2010; 88(1):45-53.
[18] Dolšek M and Fajfar P. The effect of masonry infills on the seismic response of a four-storey reinforced concrete frame - a deterministic assessment. *Engineering Structures* 2008; 30(7):1991-2001.
[19] Pagani M, Monelli D, Weatherill G, Danciu L, Crowley H, Silva V and Simionato M. OpenQuake engine: an open hazard (and risk) software for the global earthquake model. *Seismological Research Letters* 2014; 85(3):692-702.
[20] Baker JW. Conditional mean spectrum: Tool for ground-motion selection. *Journal of Structural Engineering* 2010; 137(3):322-331.
[21] Macedo L and Castro JM. SelEQ: An advanced ground motion record selection and scaling framework. *Advances in Engineering Software* 2017; 114:32–47.
[22] Ancheta TD, Darragh RB, Stewart JP, Seyhan E, Silva WJ, Chiou BSJ, Wooddell KE, Graves RW, Kottke AR, Boore DM, Kishida T, and Donahue JL. NGA-West2 Database. *Earthquake Spectra* 2014; 30(3):989-1005.
[23] Jalayer F and Cornell CA. Alternative non-linear demand estimation methods for probability-based seismic assessments. *Earthquake Engineering & Structural Dynamics* 2009; 38(8):951-972.
[24] Christovasilis IP, Cimellaro GP, Barani S and Foti S. On the selection and scaling of ground motions for fragility analysis of structures. Proceedings of the *2nd European Conference on Earthquake Engineering and Seismology* 2014; 24-29 August, Istanbul, Turkey.
[25] Grammatikou S, Biskinis D and Fardis MN. Flexural rotation capacity models fitted to test results using different statistical approaches. *Structural Concrete* 2018; 19(2):608-624.
[26] Biskinis DE, Roupakias GK and Fardis MN. Degradation of shear strength of reinforced concrete members with inelastic cyclic displacements. *Structural Journal* 2004; 101(6):773-783.
[27] Baker JW. Efficient analytical fragility function fitting using dynamic structural analysis. Earthquake Spectra 2015; 31(1):579-599.
[28] Aslani H. Probabilitistic earthquake loss estimation and loss disaggregation in buildings. Ph.D. thesis, Stanford University; 2005
[29] ASCE/SEI 41-17. Seismic rehabilitation and retrofit of existing buildings. American Society of Civil Engineers, 2017, Reston, VA
[30] Cardone, D., & Perrone, G. Damage and loss assessment of pre-70 RC frame buildings with FEMA P-58. Journal of Earthquake Engineering 2017, 21(1), 23-61.